J. Condensed Matter Nucl. Sci. 33 (2020) 111–125

Research Article

Pulsatile Superhyperfine Lines at 327.37 MHz Herald LANR Activity and Possible Mass–Energy Transfer

Mitchell R. Swartz*

JET Energy Inc., Wellesley Hills, MA 02481, USA

Abstract

Active lattice assisted nuclear reaction (LANR) systems, both aqueous and dry preloaded nanomaterials, emit very narrow bandwidth hyperfine radiofrequency (RF) emission peaks at 327.37 MHz. This is located very close to the theoretical Deuteron-Line (DL; 327.348 MHz) region. At higher applied driving voltages, a complex superhyperfine line structure of sidebands appears. At least some of their emitting RF radiation superhyperfine line peaks, heralding the inverted population, are observed to be apparently pulsing. This may be a sign of real time mass-energy transfers within the high loaded Group VIII lattice.

Keywords: Atomic deuteron, Deuterium, LANR hyperfine lines, Pulsing superhyperfine line, Superhyperfine spectra, Resonance broadening, Vacancy active site

1. Introduction – CF/LANR RF Deuterium Line Emissions

Active cold fusion/lattice assisted nuclear reactions (CF/LANR) systems, both nanomaterial [1–14] and aqueous [13–29] emit very narrow bandwidth radiofrequency (RF) emission peaks (ca. 327.37 MHz), in the Deuteron-Line (DL; 327.348 MHz) region [30]. This paper reports that within the maser spectrum are pulsatile superhyperfine RF lines (PSHFL) with periods of minutes. It is unlike everything else examined over two years from Earth and galactic origin, and only associated with XSH from an ordinary water nickel CF/LANR system. The superhyperfine sideband line (SHFL) structure (Fig. 1) has been analyzed for this aqueous nickel CF/LANR system in its active mode. It may herald quantum mechanical movements or even perforation through the Coulomb barrier.

2. Experimental

2.1. Aqueous nickel LANR system

The high Q ($> 1.2 \times 10^6$) and Zeeman response indicate maser action. There is the appearance of maser line sidebands (superhyperfine lines) with increasing voltage (Fig. 1). They appear separated by resonance broadening and energy

*Mitchell R. Swartz ScD, MD, EE, ACIER, E-mail: drswartz@nanortech.com.

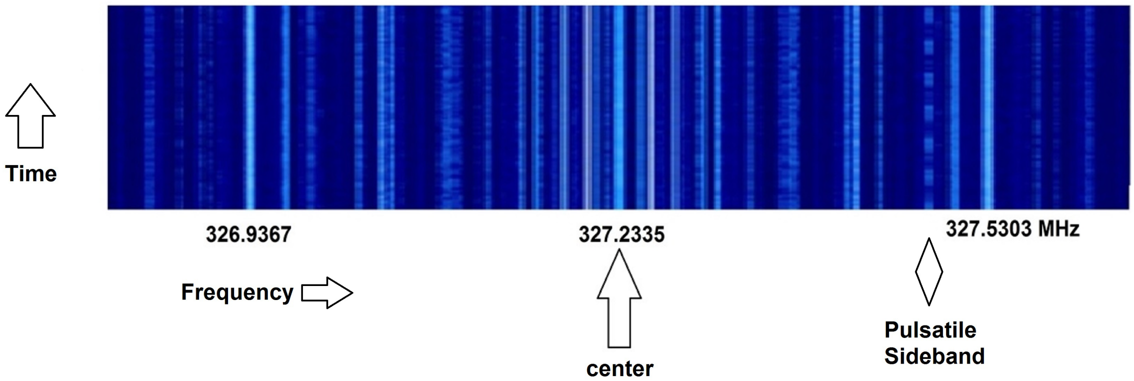

Figure 1. Pulsatile RF emissions in a background of other RF SHF lines. The radiofrequency superhyperfine DL spectrum of this nickel hydrogen loaded LANR system during its active state (40 V, 200 mA). This is a "waterfall" plot and intensity is shown as a function of frequency. Note the central arrow appears to almost be a vertical mirror along the horizontal axis. The largest amplitude pulsatile RF line is clearly visible on the right-hand side, and is marked by a star.

exchange processes [30,31]. Resonance broadening occurs when the perturbing particle is of the same type as the emitting particle and it introduces the possibility of energy exchange processes. The resonance broadening goes as $1/r^3$. The data uniquely shows the nearby sites surrounding the active site in an active nickel CF/LANR system studied. The Mother of all Cathodes (MOAC) cell has a 3 l capacity with a cathode weighing 2.132 kg (#46 hard drawn smooth nickel wire with an area of ca. 240,000 cm^2). The electrolyte was a dilute carbonate solution in laboratory distilled deionized ordinary water. These studies used Deuterium Line (DL) emissions from the MOAC LANR (ordinary water) aqueous system electrically driven during its active mode [30,31]. For the calorimetry, calibration was determined by ohmic controls and other methods, as discussed elsewhere [13–29].

2.2. Methods – RF emission detection system

The previous paper [30] discussed in detail the arrangement of detecting the RF emissions. Software defined radio (SDR) receivers were used because of their high dynamic range, high bandpass stability, and excellent out-of-band rejection. The sample rate was 3.2 million samples per second (MSPS). Upper sideband (USB) was used to minimize imaging. Resolution was the highest achievable with a Blackman– Harris 4 window, Hann or Hamming windows.

The sensitivity of this detection system (signal to noise ratio: SNR) is proportional to $A * \sqrt{t}$, where A is the antenna's collecting area, and t is the integration time. The signals are weak, and therefore the antenna is made with an aperture as large as possible, using a duck antenna system because of its easy fit into the resonance chamber. The use of antenna analyzers and matching decreased the standing wave ratio (SWR) from circa 20+ to 2 to 3. The use of military grade coax (CNT400) decreased the transmission line loss by +90 dB, and the low noise amplifier (LNA) provided an additional +20 dB gain. Ferrites are used to minimize shield currents and radio frequency interference (RFI) near active equipment.

3. Results

3.1. RF emissions from active aqueous Ni MOAC

This experimental survey began with preliminary amateur radio and LANR investigations that examined and resolved, for the first time, the apparent absence of Hydrogen Line (HL) and presence of DL emissions from the MOAC LANR (ordinary water) aqueous system electrically driven during its active mode [30,31]. The HL and DL were regions were examined with the MOAC off over weeks, to learn the galactic (followed by the zodiac) rhythm. The initial HL results were inconclusive but with recent improvements in sensitivity and selectivity, further investigations are warranted.

The DL results showed something else. Figure 2 shows these RF DL emissions from an active aqueous Ni MOAC. The figure shows the data for experiment E31=180 503 with the driving power off, and then at 10 V and 45 mA electrical current, and then at 20 V and $\sim$ 200 mA electrical current. Figure 2 is composed of three curves showing the output of an aqueous Ni/H_2OD_2O/Pt system MOAC-type, at three moments in time, at three moments in time; post-loading no further electrical input, electrical drive at the optimal operating point, and just beyond that input power. Figure 2 compares the emission in the RF region between 327.25 and 327.5 MHz (the D-line region) for the MOAC while off and while it was electrically driven at two levels (top of OOP), and just to the right of the peak. The upper curves are a brief waterfall display. The central peaks are labeled by and arrow at 327.3 MHz). The figure shows a clear comparison of the D-line RF emissions from the aqueous MOAC in three different electrical current drives; each separated by vertical lines during three different times and electrical input powers (0, 450 mW, and 4 W). The first on the left, is where MOAC was OFF. The second two were electrically driven at two input power levels. The central

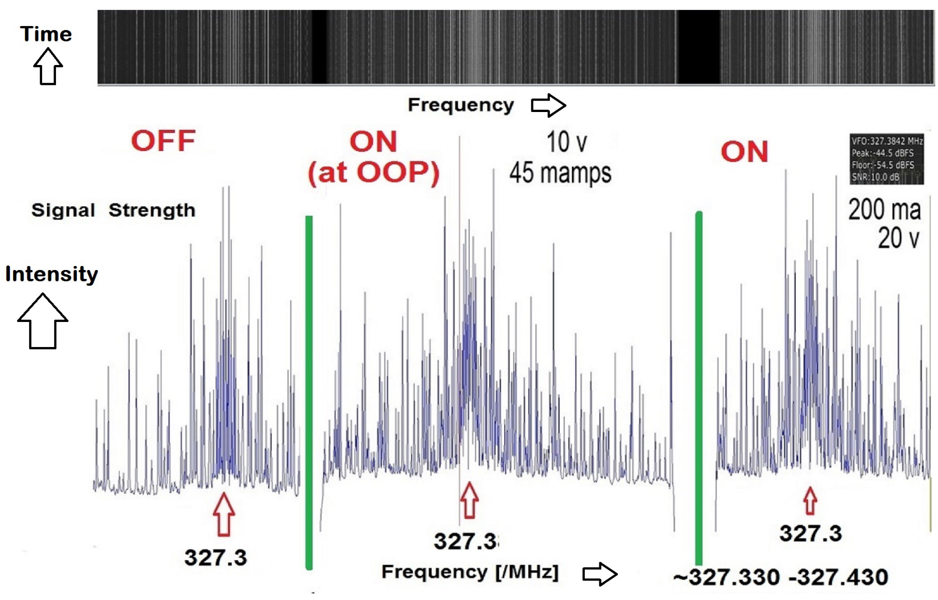

Figure 2. Comparison of the D-line RF emissions from the aqueous MOAC in three different electrical current drives; each separated by vertical lines. These focus on the region from 327.3 to 327.43 MHz (the D-line region) during three different times and electrical input powers (0, 450 mW, and 4 W) The first on the left, is where MOAC was OFF. The second two were electrically driven at two input power levels. The central curve had its electrical drive point was very close to the peak of the optimal operating point (OOP) manifold [29,15]. The increased emission in the D-Line region is apparent.

curve had its electrical drive point was very close to the peak of the optimal operating point (OOP) manifold.

Attention is directed to the fact that there are distinguishable differences in both the integrated amplitude near that region, and in the nature of the superhyperfine structure (sidebands). The increased emission in the D-line region is apparent. These sidebands are analyzed below.

Because of the positive results in the aqueous system, it was elected to further investigate the dry, preloaded NANOR®-type components for possible RF emission, too.

3.2. Pulsing deuterium line from active aqueous Ni/H_2O/Pt system

A unique pulsatile superhyperfine RF line (PSHFL) is evident with periods of minutes, and is associated with XSH from an ordinary water nickel, very large cathode, LANR system. In Figs. 1–3 are shown is the superhyperfine DL spectrum of the hydrogen loaded nickel MOAC in its active state (40 V, 200 mA).

In Fig. 1, the frequencies of the widest, and central, peaks are identified by angular frequency. The center is

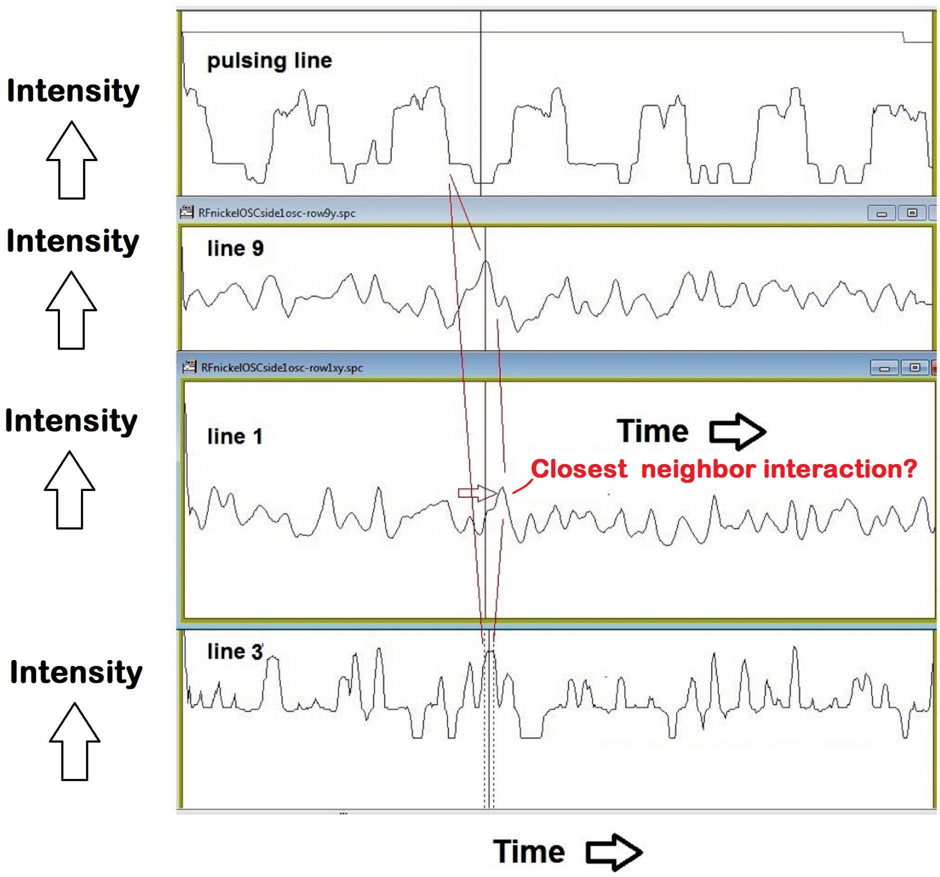

Figure 3. Amplitude of pulsatile RF line and three other time-matched RF lines.

identified by the arrow. There is very reasonable symmetry, more so than for the active electrically driven nanostructured ZrO_2–PdD [1–12]. Analysis of the amplitude and positions as a function of frequency strongly suggest that the hydride nickel has changed; perhaps a in part a phase change from a simple face centered cubic (FCC) lattice [30,31]. Attention is drawn to the pulsatile RF line.

Figure 3 shows a blow up of the pulse, and three other pulses, as function of time. What was vertical in Fig. 1 is now horizontal in Fig. 2. This shows a possible connection between some of the SHFL sidebands.

Does the deuteron density actually move to other regions during this event?

4. Interpretation

4.1. Pulsing sideband at 327.37 MHz is not mode locking

This is not mode-locking. Mode-locking was first reported by Gurs and Muller [36,37] on ruby lasers, and Statz and Tang [38] on He–Ne lasers, and reviewed by Herman Haus [39]. The author first did mode-locking experiments with a He–Ne laser in 1967 with Dr. Hermann Haus at MIT. It is the author's belief that these pulsatile densities in the RF spectrum of the 327 MHz CF/LANR maser are unlikely to be mode locking.

4.2. Background – mode locking

Mode-locking is a laser technique to create pulses of light of extremely short duration, circa picoseconds to femtoseconds. The concept of mode-locking describes enforcing coherence between multiple axial modes in a resonant laser cavity so that pulses of laser light result – observed as changes in the intensity of selected longitudinal modes. The process creates a fixed-phase relationship between modes created by the laser's chemistry and the Fabry Perot cavity. The pulses arrive in a train as the laser becomes "phase-locked" (also called "mode-locked"). Although these pulses are slower than the overall energy exchange between atoms emitting the radiation and the sea of photons in which they immersed, they are picoseconds or less. Mode-locking engineering over 6 decades has involved making the pulses shorter while increasing the understanding of the electrical engineering process.

4.3. Reason 1 – Spatial reason disproving that this is not mode locking

First, in laser mode locking, the resonant cavity's length, L, is such that it is much greater than the wavelength of the light, λ. In mode locked lasers, there are usually at least 100 half wavelengths, enabling interaction of different mode orders, i.e. n and $n+1$. Laser mode locking involves hundreds of half-wavelengths, enabling superposition of different modes (e.g. half wavelength, full wavelength, . . . , etc.). This occurs in lasers where the resonant cavity's length, L, is much greater than the wavelength of the light, λ. This is multi-mode operation.

By contrast, the 327 MHz LANR RF maser has only single-mode (half wavelength) operation. The resonant rhombic metallic box used to make the simple cavity allows modes which have the separation distance of the mirrors between 0 and L (i.e. length of the resonant box) equal to an exact multiple of half wavelengths.

4.4. Reason 2 – Temporal reason disproving that this is not mode locking

Second, in laser mode locking, the mode orders are periodically constructively interfere to create a single pulse of light. The pulses are separated in time by $\tau = 2L/c$, the time for one path back and forth across the Fabry–Perot laser cavity. By contrast, the 327 MHz LANR RF maser's unique pulsing sidebands are characterized by times which are minutes long.

4.5. Reason 3 – Pulse shape reason disproving that this is not mode locking

Third, in laser mode locking, the pulses have a Gaussian shape, although for femtosecond pulses a hyperbolic-secant-squared (sech2) pulse shape is assumed. By contrast, the 327 MHz LANR RF maser's pulses appear almost as step functions. This could however also be a result of the qualitative analysis of intensity, although it is unlikely because the RF frequency examined does not significantly change.

4.6. An intralattice kinetoscope

One important implication is that in active CF/LANR systems the loaded deuterons work together from their vacancy sites and enable the desired XSH-producing reactions within the loaded Group VIII metal while emitting RF radiation at the Deuterium-line heralding the inverted population. Is this the first intralattice movie of what occurs?

Efforts are underway to examine this further, including intensities, pulsations and transfer-movements. Taken together, they suggest a need for an intralattice kinetoscope. Two types are being examined.

4.7. Possible lattice interactions

The 327.37 MHz RF emission peaks, specifically the pulsatile superhyperfine structure may yield information of these desired reactions unlike everything examined previously. Do the pulsed RF superhyperfine bands herald one or more of these collective excitations enabling the desired reactions? It is a fact that thirty years of data demonstrate that deuterons loaded into Group VIII metals DO work together in active LANR systems to generate *de novo* ^{4}He. But how? The RF emissions show that there are inverted populations of atomic D [30] with RF D-line emission sidebands [31] and this RF pulsing from active LANR systems might indicate part of an active-necessary deuteron redistribution in the lattice.

These pulsing RF D-L bands directly herald active LANR activity. They may also herald, and allow further exploration of, deuteron (energy–mass) movements between, and to other, lattice regions, as revealed by the PSHFL (and interpreted, depending upon the model used: Band States, Bose–Einstein condensates, and other quasiparticles), including redistributions between lattice specific periodic lattice regions. Is such redistribution a *sine qua non* for successful movement through the Coulomb barrier?

4.8. Possible sign of loss of Coulomb barrier

Vladimir Dubinko has proposed Nuclear Fusion of Hydrogen Isotopes Induced by the Phason Flips in Pd and Ni nanoclusters [44]. These involve changes in the amplitude of mass–energy components giving rise to a calculated lower Coulomb barrier. The RF superhyperfine pulses, the redistribution in the RF superhyperfine spectrum, and the excess heat and antiStokes observed support his theory.

4.9. Implications of d-line shfl pulsing discovery

4.9.1. *Detection of ion band states, Bose–Einstein states, or Phusons?*

In one way, this is retrospectively even expected. Unlike quasiparticles, collective excitations result from the ORGANIZED aggregate behavior of the object (usually a lattice). A coherent collective excitation is one which is united and forms an entire uniform constant phase relationship. The pulsing RF signal may be that. It may reveal some of those factors that contribute to increase the likelihood of possible fusion. These might include electrical charging of the cathode to a high negative voltage, or the deuteron or ion band structure, or Bloch-symmetric Bose–Bloch condensates

[40–43], or plasmon exchange, or electron screening, or the increased effective mass of the deuterons due to polarons which occur in the crystalline lattice and other dielectrics used. They may also be tied to Phusons (***) [34,35], or other reported/theoretical ideas in CF/LANR used to enable successful movement through the Coulomb barrier, and therefore towards successful CF/LANR.

These other theoretical ideas include Lou Dechiaro's recognition of coherence among self-sustained maser longitudinal modes in a CF/LANR system which might well related to the Fourier components of the nuclear quantum wavefunctions as taught by Vyssotsky, Adamenko, and Dubinko.

4.9.2. *Detection of Coulomb barrier loss?*

It may be that such resonance(s) involving wavefunction coherence, as now detected [30,31], may also lead to quantum mechanical movements, perhaps even along with the disappearance of the Coulomb barrier under the right conditions (ICCF22 [44]).

4.10. Phuson theory (***)

The Phuson theory incorporates the observed products and the energy levels, and explains the branching ratios based on the thermal energies available [34]. It also explains the origin of the excess heat in active LANR systems. In addition, it explains why there is a relative absence of strong neutron and gamma ray emissions in LANR. The gamma emission branch from the excited state of ^{4}He* is actually spin-forbidden for both hot and cold fusion. However, at higher hot fusion temperatures the restriction is lifted slightly so that some gammas are seen, and not zero. This spin-forbiddenness of gamma emission is therefore consistent to what is seen for both hot and cold fusion. The Phuson theory also correctly describes the relative absence of neutrons emissions in LANR.

The only nuclear branches available are those whose band gaps are surmountable by the available activation energy (limited by the ambient temperature and incident radiation). The neutron emission branch is more than 1 MeV above the first excited state (^{4}He*). Hot fusion has large activation energies available (it is hot). LANR does not. In LANR, given the actual much smaller amount of thermal energy, $k_{\mathrm{B}} * T$ available for LANR ($\sim 1/25$ eV), absence of adequate activation energy decisively means that the branch is NOT available, as it is for hot fusion. There results: lattice heating (excess heat) and de novo ^{4}He. Neutrons are not observed, helium 4 production is in its stead [34,15].

5. Conclusion

5.1. RF findings summary

(1) Active CF/LANR systems, both aqueous and nanomaterial, emit very narrow bandwidth RF emission peaks (ca. 327.37 MHz), in the DL; 327.348 MHz region [30]. The high $Q(> 1.2 \times 10^6)$ and Zeeman response indicate maser action.

(2) There is the appearance of maser line sidebands (superhyperifine lines) with increasing voltage. They appear by resonance broadening and energy exchange processes [30,31]. Resonance broadening occurs when the perturbing particle is of the same type as the emitting particle and it introduces the possibility of energy exchange processes. The resonance broadening goes as $1/r^3$. The data uniquely show the nearby sites surrounding the active site in an active nickel CF/LANR system. The superhyperfine sideband line (SHFL) structure (Fig. 1) has been analyzed for the aqueous nickel MOAC system in its active mode [31].

(3) We report this unique pulsatile superhyperfine RF line (PSHFL) with periods of minutes. It is unlike everything else examined over two years from Earth and galactic origin, and only associated with XSH from an ordinary water nickel CF/LANR system.

(4) These pulses are not the result of mode locking. Laser mode locking involves hundreds of half-wavelengths, enabling interaction of different mode orders; but this 327 MHz LANR maser has only single-mode (half wavelength) operation. Laser mode locked pulses are separated by the Fabry–Perot cavity transit time but the 327 MHz LANR maser pulsing sideband is characterized by times which are minutes. Finally, laser mode locked pulses have a Gaussian or a hyperbolic-secant-squared (sech2) pulse shape but the 327 CF/LANR maser's pulses appear as near step functions.
(5) It may herald quantum mechanical movements or even perforation through the Coulomb barrier.

5.2. Complete LANR model based on RF LANR findings

The complete model involves the saturation of the Pd by D. This is the expected full amount that can be contained therein, and is a function of temperature. The fractional saturation and its interactions with the phonons and the interstitials and vacancies within the palladium better explain how LANR works. Simply put, there is injection of deuterons into the vacancies by the sudden catastrophic desaturation of highly loaded Pd. That is followed by a quasiparticle which drives the desired reaction by coupling to the lattice.

The firsts step is that successful LANR begins with loading of the lattice, the kinetics of which can be described by the quasi-1-dimensional model of loading [16,19,31,32]. LANR, after loading, then has at least two coherent excitation/quasiparticles in its successful action. These sections will describe the pathway to successful activity in LANR. What is described here is a multistep process to LANR. Then there occurs a coherent excitation involving the catastrophic active media forming deuteron flux and very rapidly filling of the vacancies (CAM theory). Under some circumstances, as discussed by Takahashi, Scott and Talbot Chubb and others, there can occur in the lattice the formation of *de novo* helium 4 (^{4}He*). Finally, in the fourth irreversible step there is the de-excitation through the PHUSON coherent particle [34,35]. These steps, and the energy levels explain the observations of LANR – including the excess heat, and the lack of significant emissions.

5.3. Quasi-one-dimensional loading model

As discussed at ICCF-4, we suggest a series of reversible reactions which lead up to a final irreversible step. The series includes an intermediate state which is called apo-^{4}He* (meaning that which occurs before the ^{4}He* is seen). apo-^{4}He* is on the way to becoming the excited helium state, ^{4}He*, located about 22 MeV above the ground state of helium. If the conditions are perfect, ^{4}He* can then become *de novo* ^{4}He and heat the lattice, where it appears as excess heat. If successful, then in the highly loaded lattice (n D within the Pd, which is ignored in this equation):

The LANR reaction begins in the extremely difficult-to-achieve highly-loaded Group VIII lattice. There is a critical content of loaded Pd for activity, generally described as a requirement of $>\sim 0.85$ [15]. Understanding this system requires continuum electromechanics as well as electrochemistry.

5.4. Loading requires positive deuteron flux

Deuteron flux is examined here by the quasi-1-dimensional model of loading which shows that conventional electrolysis is WRONG and a red herring, and is why many have trouble achieving successful LANR. The quasi-1-dimensional equations [32,33] also show the way to optimal results. These equations explain some of the difficulties from 1989 on, and they DO NOT DEPEND upon equilibrium conditions, and in fact they make successful predictions (both unlike the relatively useless Nernst equation). There are several components of deuteron flux. They must be considered, including entry into the metal (J_{E}), movement to gas evolution (J_{G}), and an extremely tiny loss by potential fusion reactions (J_{F}). J_{IP} is a pathway afforded by the high impedance spiral PHUSOR®-type LANR component (not to be confused with the PHUSON).

At the cathodic metal surface, several components of deuteron flux must be considered; entry into the metal (J_{E}), movement to gas evolution (J_{G}), and an extremely tiny loss by potential fusion reactions (J_{F}). J_{IP} is a pathway afforded with a metamaterial [22].

$$J_{\mathrm{D}} = B_{\mathrm{D}} \frac{\mathrm{d}[D(z,t)]}{\mathrm{dz}} - \mu_{\mathrm{D}}[D(z,t)] \frac{\mathrm{d}\Phi}{\mathrm{d}z}. \tag{1}$$

Equation (1) describes the flow. J_{D} is the flux of deuterons, B_{D} is their diffusivity, and μ_{D} is their electrophoretic mobility. The deuterons can enter the metal forming a binary alloy. Deuterons which enter (load) into the palladium lattice drift from shallow to deeper sites within the palladium, obstructed by ordinary hydrogen at interfaces and grain boundary dislocations. The quasi-1-dimensional model begins with the Navier-Stokes equations which describe flow for fluids and other materials in continuum electrodynamics [45]. Dividing each flux by the local deuteron concentration yields the first order deuteron flux constants, k_{E}, k_{G}, and k_{F} (cm/s), respectively. They are linked as follows through Gauss' law and integral equations.

$$k_{\mathrm{E}} = (\mu_{\mathrm{D}} * E) - (k_{\mathrm{G}} + k_{\mathrm{F}}). \tag{2}$$

This shows absolutely clearly that LANR can be missed by insufficient loading, contamination (affecting k_{E}, e.g. by protium), and by the evolution of D_2 gas, which all inhibit the desired reactions. This also shows that the first order deuteron loading rate equation teaches that the deuteron gain by the lattice depends on the applied electric field MINUS the loss of deuterons from gas evolution (k_{G}) and fusion (k_{F}). (consistent with conservation of mass).

Furthermore, when the deuteron flux equation is modified by the Einstein relation, the first term now has geometric, material factors, and the ratio of two energies [the applied electric energy organizing the deuterons divided by $k_{\mathrm{B}}T$, thermal disorder). The modified deuteron flux equation reveals how competitive gas evolving reactions destroy the desired reactions, and how the ratio of the applied electric field energy to thermal energy ($k_{\mathrm{B}} * T$) are both decisive in successful LANR experiments [21,15].

Step 1: (A reversible step) Loading of palladium by deuterons

$$k_{\mathrm{E}} = \frac{B_{\mathrm{D}} * qV}{L[k_{\mathrm{B}} * T]} - (k_{\mathrm{G}} + k_{\mathrm{F}}). \tag{3}$$

5.5. Catastrophic Active Medium driven deuterons and Anderson focusing

The next key movements on the road to successful cold fusion (i.e. LANR) begin with the D within the highly loaded Pd. The deuterons are driven by catastrophic desaturation following local temperature increase. This desaturaton and the rise time to produce by positive feedback are described by the CAM (catastrophic active media) model. Briefly, after loading (Step 1), there can –under some conditions – occur Step 2 which is the CAM-driven filling of vacancies.

Step 2: (A reversible step) CAM formation of apo-*He^4 in hyperloaded vacancies

$$\mathrm{D} + \mathrm{D}(\text{observed via pulsatile quantum action}) \rightleftarrows {}^4\mathrm{He}^*. \tag{4}$$

In summary, the CAM reactions drive the loaded deuterons to the vacancy sites. Catastrophic Active Medium (CAM) model [16] of LANR considers the deuteron solubility in, and the unusual solubility–temperature relationship with, palladium. Unlike most metals characterized by low solubility (∼one deuteron per 10,000 metal atoms), the deuteron solubility in palladium is quite large and decreases with temperature.

Takahashi has denoted that clusters of 4 and 6 may especially enable these desired reactions. The CAM model first treats the metallic Pd lattice, into which isotopic fuel is loaded, like a vase for the D (emphore, from *amphora*), and follows the changes in partial saturation of the Pd with D.

Second, the model adds in the fact that the Pd is an active medium capable of rapid desorption of deuterons, thus with recruitment potential of even more deuterons. This can happen in a paroxysmal and catastrophic way with feedback effects. This has a profound impact on increasing deuteron recruitment, which means the increase of heat produces even more suddenly available deuterons by desorption of D from the Pd (positive feedback [46]). Third, the model reflects that the metallic Pd lattice is heterogeneous, and the model considers *all* types of sites in which the intraelectrode deuterons can reside, including deeper traps supplementing the octahedral and tetrahedral sites. Most importantly, the model documents that the loaded Pd is an active medium capable of rapid deuteron desorption and redistribution (shown in Fig. 4 by τ_{C}), and that there can also be movements into vacancies, and Anderson focusing (a solid state effect which focuses D flux into vacancies).

It is the movement of deuterons from throughout the loaded palladium to the active sites that begins the LANR process, and it is augmented by feedback, by phonon-flux coupling, and by the confinement (discussed in the CAM theory from ICCF-4 when the nuclear active site was first introduced). A partial CAM computer model (from ICCF-4) relating the normalized deuteron fugacity, temperature, and the fractional saturation (Fig 4) shows the relationship of loading, deuterium, and temperature within the cathode. This has been shown to be qualitatively consistent with some experimental observations, as confirmed by Martin Fleischman after ICCF-4.

The model shows that although the deuteron fugacity ($\Theta_{\mathrm{D,Pd}}$) (where fugacity is related to the deuteron pressure rises slightly, thereafter the deuteron saturation curve in Fig. 4 falls rapidly for the loaded palladium. There is a 7-fold decrease in content from 5 to 50°C. Prior to destruction of the lattice through cracks and dislocations and rupture, this desaturation creates an increase in the intrinsic pressure (fugacity) which follows the intraelectrode deuteron flux from redistribution. Because of the fractional saturation-temperature effect, dynamic inversion of $\Gamma_{\mathrm{D,Pd}}$ (t) occurs as

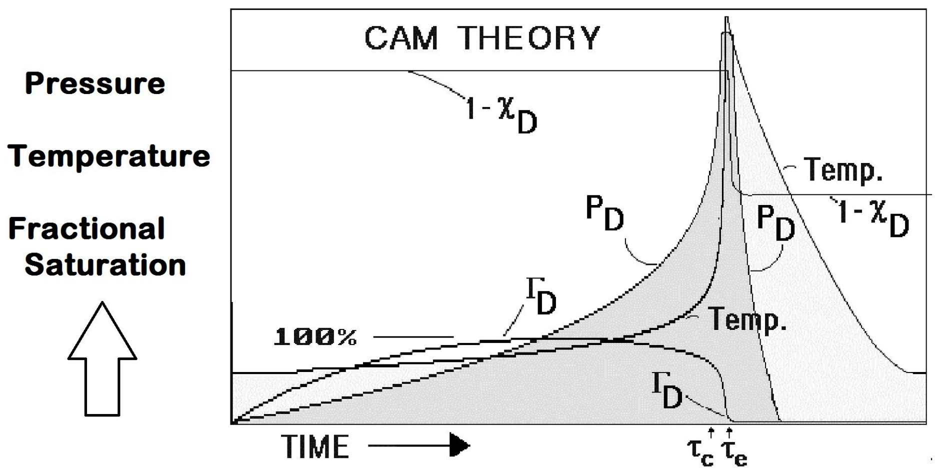

Figure 4. Catastrophic redistribution of deuterons (described by CAM theory). Temperature and loading as a function of time – the theoretic results of a sudden CAM desaturation of a palladium electrode with respect to deuterons. As the palladium heats up (in positive feedback), the solubility of the D in it decreases, leading to a massive falloff of the fractional saturations (D/(PdD) % defined as Γ_{D}). This drives the deuterons by the CAM catastrophic desaturation into the vacancies which are the site of the LANR reactions.

$\Theta_{\mathrm{D,Pd}}\,(t)$ and temperature reach crescendo levels. As a result, after sufficient time, the active site (compartment 2) is suddenly and catastrophically fed deuterons from the large vicinal volumes of the crystalline palladium lattice (compartment 1), further increasing the likelihood of additional temperature-incrementing reactions. Eventually, however, the crystal lattice is unable to survive intact, and instead the surface energy normally is required to prevent the palladium from escaping, becomes insufficient and the reactants continue to move from their normal sites to accumulate in compartment 2 by the catastrophic reactions and thereby maintain close contact for the desired reactions.

The surface energy required to rupture the palladium prevents the escape of the reactants as they continue to accumulate by the catastrophic reactions and thereby maintain close contact for the desired reactions. Positive feedback comes from the catastrophic behavior secondary to the saturation-temperature relationship. However, when the internal pressures are able to exceed the energy needed to create fresh new surfaces in the palladium, leakage then occurs and the sample becomes, at best, locoregionally inactive.

5.6. Phusons and successful LANR

The lattice enables this reversible reaction through internal conversion [40–43]. The critical reaction proceeds and is described by either band states and/or Bose–Einstein states, and other interaction models. It is enabled by the collective excitations of phonons. In addition, it is reasonable to assume that conditions may enable formation of ^{4}He* if and when there is sufficient activation energy [27, 47–49].

Looking closer at the phonons and their role: Cold fusion is enabled by the collective excitations of phonons. After adequate containment time and flux, there is near commensurate amount of excess heat observed in LANR, with the ash which is *de novo* He^4. Phonon de-excitation modes apparently produce transitional times significant for enabling ^{4}He* to ^{4}He transitions which involving recruitment of sufficient numbers of lattice sites and their associated phonons. The temperature rise occurs as the acoustical and optical phonons are eventually unable to carry off all the momentum and the excess energy of the reactions appears and grows. This process is the unique feature that allows LANR to occur with energy transfer to the lattice which does enable the desired reactions if and when there is sufficient activation energy [27,47–49] The penultimate critical ($\sim$ 20 MeV) transition shown above is enabled by the coherent Phuson, enabled by phonons, Hagelstein's lossy spin bosons, and magnons [9,15]. Hagelstein incorporates the optical phonons in his theory. Swartz at ICCF20 has shown these to also, obvious by coherent antiStokes spectroscopy, include acoustic phonons [11,12,18].

5.7. Phuson quasiparticle enables coherent collective de-excitation

The pulsing RF superhyperfine bands interacting may be the Phuson quasiparticle. The coherent means of excitation of the lattice, the Phuson [34,35], enables LANR by coherent transfer of energy from ^{4}He* to the lattice in a process which is consistent with conventional physics, and where it appears as excess heat [15] and *de novo* ^{4}He. As discussed in the original paper, the PHUSON theory has a mechanism which incorporates the observed products, and the energy levels to all those branches. As a result, it succinctly explains the differences in observed outputs, including the observed excess heat as T rises. It also explains the different branches observed near room temperature (LANR) and at hot fusion temps. The temperature rise occurs as the acoustical and optical phonons become unable to carry off all the momentum and excess energy of the reactions. In this step (Step 3), there is a critical IRREVERSIBLE (~ 20 MeV) transition that is coherent by PHUSON, enabled by phonons and magnons. The Phuson is a coherent particle of the lattice. Simply put, the Phusons, coherent excitation objects/particles cooperatively transfer energy from the megavoltage energy of the ^{4}He* to the lattice.

Step 3: (An irreversible step) de-excitation by Phuson/Phonons (in lattice) to He^4

$$\begin{aligned} {}^4\mathrm{He}^*[\text{via PHUSON-coherent transfer}] &= (*) \Rightarrow\ {}^4\mathrm{He} \\ (*)\ \text{requires phonons and magnons} \end{aligned} \tag{5}$$

The coherent de-exciting PHUSON enables the massive energy loss by way of lossy spin bosons processes involving phonons and (as we have shown at ICCF-18) magnons. There are many factors that contribute to increase the likelihood of possible fusion: electrical charging of the cathode to a high negative voltage, the deuteron band structure, Bloch-symmetric Bose–Bloch condensates, plasmon exchange, electron screening, and the increased effective mass of the deuterons due to polarons which occur in the crystalline lattice and other dielectrics used.

6. Conclusions

6.1. LANR RF emission summary

Active CF/LANR systems, both aqueous and nanomaterial, emit very narrow bandwidth hyperfine RF emission peaks (ca. 327.37 MHz), which are located very close to the theoretical DL; 327.348 MHz) region, and they exhibit a large $Q(> 1.2 \times 10^6)$, which is the ratio of the bandwidth at half power to the frequency. RF identification and recognition of CF/LANR RF emission from the active state is important. In the future, RF detection, like coherent antiStokes spectroscopy [11–13,18] can be used, aimed at the phenomenon's location, to discern the conditions of the desired active XSH-producing driven state.

6.2. Confirmation of fuel – Deuterons free radicals

These results confirm that in active CF/LANR systems deuterons are making helium-4 which generates the observed excess energy in the active state [50,17].

6.3. Derivation of the active site – FCC vacancies

At higher applied driving voltages, a superhyperfine line structure of sidebands appears, and that this revelation gives more insight into the volume and stereoconstellation around the active site. The fuel generates the fusion product and at least some of these reactions occur in face center cubic (Pd FCC) vacancy for palladium (in PdD) or Zr (in ZrO_2). Vacancies, as predicted at ICCF-4 [46], are the site of some of the desired reaction in these active systems.

6.4. Real time mass–energy intralattice spectroscopy

In active CF/LANR systems, the loaded deuterons work together from their vacancy sites to enable continuation of the desired XSH-producing reactions within the loaded Group VIII metal. At least some of their emitting RF radiation superhyperfine line peaks, located at the DL heralding the inverted population, are observed to be pulsing. This action may herald quantum movements of energy and matter within an active XSH-producing PdD lattice. With the new information derived from the RF superhyperfine pulsing data and analysis, one can uncover where the highest energy precursor to the final state spatially occurs and observe in real time mass-energy transfers within the high loaded Group VIII lattice.

Acknowledgments

The author gratefully acknowledges and thanks David Nagel, Bo Gardmark, Gayle Verner, Peter Hagelstein, Lawrence Forsley, Louis Dechiaro, Isidor Straus, and Joshua Gyllinsky for their very helpful comments, editorial assistance, and additional material. He also thanks Brian Ahern, Alan Weinberg and the late Charles W. Haldeman for their construction, early testing, and transfer of the MOAC. This effort has been supported by JET Energy Inc., Nanortech Inc., and the Anthropocene Institute, LLC.

References

[1] M.R. Swartz, G. Verner and J. Tolleson, Energy gain from preloaded ZrO_2–PdNi–D nanostructured CF/LANR quantum electronic components, *J. Condensed Matter Nucl. Sci.* **13** (2014) 528, www.iscmns.org/CMNS/JCMNS-Vol13.pdf.

[2] M.R. Swartz, G. Verner, J. Tolleson and P.L. Hagelstein, Dry, preloaded NANOR®-type CF/LANR components, *Current Sci.* **108** (4) (2015) 595.

[3] M.R. Swartz and P.L. Hagelstein, Demonstration of energy gain from a preloaded ZrO_2–PdD nanostructured CF/LANR quantum electronic device at MIT, *J. Condensed Matter Nucl. Sci.* **13** (2014) 516, www.iscmns.org/CMNS/JCMNS-Vol13.pdf.

[4] M.R. Swartz, P.L. Hagelstein and G. Verner, Impact of electrical avalanche through a ZrO_2–NiD nanostructured CF/LANR component on its incremental excess power gain, ICCF-19, *J. Condensed Matter Nucl. Sci.* **19** (2016) 287–297.

[5] M.R. Swartz, Optical detection of phonon gain distinguishes an active cold fusion/LANR component, *J. Condensed Matter Nucl. Sci.* **20** (2016) 29–53, www.iscmns.org/CMNS/JCMNS-Vol20.pdf.

[6] M.R. Swartz and P.L. Hagelstein, Increased PdD anti-Stokes peaks are correlated with excess heat mode, *J. Condensed Matter Nucl. Sci.* **24** (2017) 130–145.

[7] M.R. Swartz, G. Verner, J. Tolleson, L. Wright, R. Goldbaum and P.L. Hagelstein, Imaging of an active NANOR®-type LANR component using CR-39, *J. Condensed Matter Nucl. Sci.* **15** (2015) 81.

[8] M.R. Swartz, Incremental high energy emission from a ZrO_2–PdD nanostructured quantum electronic component CF/LANR, *J. Condensed Matter Nucl. Sci.* **15** (2015) 92.

[9] M.R. Swartz, G. Verner, J. Tolleson, L. Wright, R. Goldbaum and P.L. Hagelstein, Amplification and restoration of energy gain using fractionated magnetic fields on ZrO_2–PdD nanostructured components, *J. Condensed Matter Nucl. Sci.* **15** (2015) 66, www.iscmns.org/CMNS/JCMNS-Vol15.pdf.

[10] M.R. Swartz, P. Hagelstein and G. Verner, Impact of electrical avalanche through a ZrO_2–NiD nanostructured CF/LANR component on its incremental excess power gain, ICCF-19, *J. Condensed Matter Nucl. Sci.* **19** (2016) 287–297.

[11] M.R. Swartz, Optical detection of phonon gain distinguishes an active cold fusion/LANR component, *J. Condensed Matter Nucl. Sci.* **20** (2016) 29–53, www.iscmns.org/CMNS/JCMNS-Vol20.pdf.

[12] M.R. Swartz and P.L. Hagelstein, Increased PdD anti-stokes peaks are correlated with excess heat mode, *J. Condensed Matter Nucl. Sci.* **24** (2017) 130–145.

[13] M.R. Swartz, Aqueous and nanostructured CF/LANR systems each have two electrically driven modes, *J. Condensed Matter Nucl. Sci.* **29** (2019) 177.

[14] M.R. Swartz, Comparison of NANOR®-type LANR components to ^{238}Pu as a heat source for space flight, *J. Condensed Matter Nucl. Sci.* **29** (2019) 238.

[15] M.R. Swartz, Survey of the observed excess energy and emissions in lattice assisted nuclear reactions, *J. Sci. Exploration* **23** (4) (2009) 419–436.

[16] M.R. Swartz, Excess power gain using high impedance and codepositional LANR devices monitored by calorimetry, heat flow, and paired stirling engines, *Proc. ICCF* 14, **1** (2008) 123; ISBN: 978-0-578-06694-3, 123, (2010); www.iscmns.org/iccf14/ProcICCF14a.pdf.

[17] M.R. Swartz, Charles Haldemann, Alan Weinberg and Brian Ahern, Possible deuterium loss during excess heat from ordinary water-carbonate electrolyte using nickel, *J. Condensed Matter Nucl. Sci.* **29** (2018) 169.

[18] M.R. Swartz, Increase of an anti-Stokes peak at the cathode of an electrically-driven, active aqueous nickel/H_2O/Pt system, *J. Condensed Matter Nucl. Sci.* **29** (2018) 22.

[19] M.R. Swartz, Consistency of the biphasic nature of excess enthalpy in solid state anomalous phenomena with the quasi-1-dimensional model of isotope loading into a material, *Fusion Technol.* **31** (1997) 63–74.

[20] M.R. Swartz, Codeposition of palladium and deuterium, *Fusion Technol.* **32** (1997) 126–130.

[21] M.R. Swartz and G. Verner, Excess heat from low electrical conductivity heavy water spiral-wound Pd/D_2O/Pt and Pd/D_2O-

$PdCl_2$/Pt devices, Condensed matter nuclear science, *Proc. ICCF*-10, World Scientific, NJ, ISBN 981-256-564-6, 29-44; 45–54 (2006).

[22] M.R. Swartz and G. Verner, The Phusor®-type LANR cathode is a metamaterial creating deuteron flux for excess power gain, *Proc. ICCF*-14, **2** (2008) 458, ISBN: 978-0-578-06694-3, 458 (2010).

[23] M.R. Swartz, G. Verner and A. Weinberg, Non-thermal near-IR emission from high impedance and codeposition LANR devices, *Proc. ICCF* 14, D.J. Nagel and M.E. Melich (Eds.), **1** (2008) 343, ISBN: 978-0-578-06694-3, 343, (2010), www.iscmns.org/iccf14/ProcICCF14a.pdf.

[24] M.R. Swartz, Improved electrolytic reactor performanceusing π-notch system operation and gold anodes, transactions of the American nuclear association, Nashville, Tenn. Meeting, (ISSN:0003-018X publisher LaGrange, Ill) **78** (1998) 84–85.

[25] M.R. Swartz, Can a Pd/D_2O/Pt Device be Made Portable to Demonstrate the Optimal Operating Point? Condensed Matter Nuclear Science, *Proc. ICCF-10*, P.L. Hagelstein and S.R. Chubb (Eds.), World Scientific, NJ, ISBN 981-256-564-6, 29-44; 45–54 (2006).

[26] M.R. Swartz, Investigations of heat after death, *J. Condensed Matter Nucl. Sci.* **31** (2020) 20–41.

[27] M.R. Swartz, Photoinduced excess heat from laser-irradiated electrically-polarized palladium cathodes in D_2O, Condensed Matter Nuclear Science, *Proc. ICCF*-10, NJ, ISBN 981-256-564-6, 213-226 (2006).

[28] M.R. Swartz, G. M. Verner and A.H. Frank, The impact of heavy water (D_2O) on nickel-light water cold fusion systems, *Proc. ICCF* 9, China, Xing Z. Li (Ed.), May 2002, pp. 335–342.

[29] M.R. Swartz, optimal operating point manifolds in active, loaded palladium linked to three ditinct physical regions, *Proc. ICCF*14 , D.J. Nagel and M.E. Melich (Eds.), Vol. 2, 2008, p. 639, ISBN: 978-0-578-06694-3, 639, (2010).

[30] M.R. Swartz, Deuterons in active LANR systems emit a327.37 MHz hyperfine maser line, *J. Condensed Matter Nucl. Sci.* (2019), to apear.

[31] M.R. Swartz, Superhyperfine line structure of ZrO_2PdD RF emission heralds a deuteron in a FCC vacancy, *J. Condensed Matter Nucl. Sci.* (2019), to appear.

[32] M.R. Swartz, Quasi-one-dimensional model of electrochemical loading of isotopic fuel into a metal, *Fusion Technol.* **22** (2) (1992) 296–300.

[33] M.R. Swartz, Isotopic fuel loading coupled to reactions at an electrode, *Proc. ICCF*4 **2** (1993) 429, *Fusion Technol.* **26** (4)T (1994) 74–77.

[34] M.R. Swartz, Phusons in nuclear reactions in solids, *Fusion Technol.* **31** (1997) 228–236.

[35] M.R. Swartz, Quasiparticles, collective excitations and higher-order collective quasi-excitations in lattice assisted nuclear reactions, *J. Condensed Matter Nucl. Sci.* with excess heat mode, *J. Condensed Matter Nucl. Sci.* **24** (2017) 130–145.

[36] K. Gurs and R. Muller, Breitband-modulation durch Steuerung der emission eines optischen masers (Auskopple-modulation), *Phys. Lett.* **5** (1963) 179–181.

[37] K. Gurs, Beats and modulation in optical ruby lasers, in *Quantum Electronics* Ill, P. Grivet and N. Bloembergen (Eds.), Columbia University Press, New York, 1964, pp. 1113–1119.

[38] H. Statz and C.L. Tang, Zeeman effect and nonlinear interactions between oscillating laser modes, in *Quantum Electronics* Ill, P. Grivet and N. Bloembergen (Eds.), Columbia University Press, New York, 1964, pp. 469–498.

[39] H.A. Haus, Mode-locking of lasers, *IEEE J.* on selected topics in *Quantum Electronics*, Vol. 6, No. 6, November/December 2000, p. 1173.

[40] T.A. Chubb and S.R. Chubb, *Ion Band States: What they are, and How they Affect Cold Fusion*, Cold Fusion Source Book, ibid., 75, (1994).

[41] T.A. Chubb and S.R. Chubb, The role of hydrogen ion band states in cold fusion, *Trans. Fusion Technol.* **26**(4T) (1994) 414.

[42] T.A. Chubb and S.R. Chubb, An explanation of cold fusion and cold fusion by-products, based on lattice induced nuclear chemistry, in *Second Annual Conference on Cold Fusion, The Science of Cold Fusion*, Como, Italy, Societa Italiana di Fisica, Bologna, Italy, 1991.

[43] T.A. Chubb and S.R. Chubb, Bloch-symmetric fusion in PdD_x, *Fusion Technol.* **17** (1990) 710.

[44] V. Dubinko, Nuclear fusion of hydrogen isotopes induced by the phason flips in Pd and Ni, *J. Condensed Matter Nucl. Sci.* (2019), to appear.

[45] J. Melcher, *Continuum Electromechanics*, MIT Press, Cambridge, 10. 13-10. 18 (1981).
https://www.google.com/url?sa=t&rct=j&q=&esrc=s&source=web&cd=4&cad=rja&uact

=8&ved=2ahUKEwj8pc7XrIjjAhVorlkKHfQjBI4QFjADegQIBhAC&url=https%3A%2F%2Focw.mit.edu%2Fans7870%2Fresources%2Fmelcher%2Fresized%2Fcem_811.pdf&usg=AOvVaw1ityC4BWlIPTM792pP5DX7.

[46] M.R. Swartz, Catastrophic active medium (CAM) theory of cold fusion, *Proc. ICCF* 4, **4** (1993) 255, sponsored by EPRI and the Office of Naval Research.

[47] D. Cravens, D. Letts and P.L. Hagelstein (Progress on two-laser experiments, *Proc. ICCF* 15 (2009); http://lenr-canr.org/acrobat/Hagelsteinprogresson.pdf) deuterium-heavy water system*, Electroanal. Chem*. **287** (1990) 293.

[48] D.Letts and D. Cravens, Laser stimulation of deuterated palladium: past and present, *Proc. 10th Int. Conf. on Cold Fusion,* 2003.

[49] D. Letts and P.L. Hagelstein, Stimulation of optical phonons in deuterated palladium. in *ICCF-14 Int. Conf. on Condensed Matter Nucl. Sci.,* 2008, Washington, DC, D. Letts, D. Cravens and P.L. Hagelstein (Eds.), *Thermal Changes in Palladium Deuteride Induced by Laser Beat Frequencies, in Low-Energy Nuclear Reactions* Sourcebook, J. Marwan and S. Krivit (Eds.), 2008, Oxford University Press, Oxford, D. Letts and D. Cravens, Laser stimulation of deuterated palladium: past and present, in *Tenth Int. Conf. on Cold Fusion,* 2003, Cambridge, MA.

[50] M. Miles, correlation of excess power and helium production during D_2O and H_2O electrolysis using palladium cathodes, *J. Electroanal. Chem*. **346** (1993) 99–117.